

## ESO Imaging Survey<sup>★</sup>

### IV. Multicolor analysis of point-like objects toward the South Galactic Pole

S. Zaggia<sup>1,2</sup>, I. Hook<sup>1</sup>, R. Mendez<sup>1,3</sup>, L. da Costa<sup>1</sup>, L.F. Olsen<sup>1,4</sup>, M. Nonino<sup>1,5</sup>, A. Wicenec<sup>1</sup>, C. Benoist<sup>1,6</sup>, E. Deul<sup>1,7</sup>, T. Erben<sup>1,8</sup>, M.D. Guarnieri<sup>1,9</sup>, R. Hook<sup>10</sup>, I. Prandoni<sup>1,11</sup>, M. Scodeggio<sup>1</sup>, R. Slijkhuis<sup>1,7</sup>, and R. Wichmann<sup>1,12</sup>

<sup>1</sup> European Southern Observatory, Karl-Schwarzschild-Str. 2, D-85748 Garching b. München, Germany

<sup>2</sup> Osservatorio Astronomico di Capodimonte, via Moiariello 15, I-80131 Napoli, Italy

<sup>3</sup> Cerro Tololo Inter-American Observatory, Casilla 603, La Serena, Chile

<sup>4</sup> Astronomisk Observatorium, Juliane Maries Vej 30, DK-2100 Copenhagen, Denmark

<sup>5</sup> Osservatorio Astronomico di Trieste, Via G.B. Tiepolo 11, I-31144 Trieste, Italy

<sup>6</sup> DAEC, Observatoire de Paris-Meudon, 5 Pl. J. Janssen, F-92195 Meudon Cedex, France

<sup>7</sup> Leiden Observatory, P.O. Box 9513, 2300 RA Leiden, The Netherlands

<sup>8</sup> Max-Planck Institut für Astrophysik, Postfach 1523, D-85748 Garching b. München, Germany

<sup>9</sup> Osservatorio Astronomico di Pino Torinese, Strada Osservatorio 20, I-10025 Torino, Italy

<sup>10</sup> Space Telescope – European Coordinating Facility, Karl-Schwarzschild-Str. 2, D-85748 Garching b. München, Germany

<sup>11</sup> Istituto di Radioastronomia del CNR, Via Gobetti 101, I-40129 Bologna, Italy

<sup>12</sup> IUCAA, Post Bag 4, Ganeshkhind, Pune 411007, India

Received July 17; accepted December 16, 1998

**Abstract.** This paper presents preliminary lists of potentially interesting point-like sources extracted from multicolor data obtained for a 1.7 square degree region near the South Galactic Pole. The region has been covered by the ESO Imaging Survey (EIS) in  $B$ ,  $V$  and  $I$  and offers a unique combination of area and depth. These lists, containing a total of 330 objects nearly all brighter than  $I \sim 21.5$ , over 1.27 square degrees (after removing some bad regions), are by-products of the process of verification and quality control of the object catalogs being produced. Among the color selected targets are candidate very low mass stars/brown dwarfs (54), white-dwarfs (32), and quasars (244). In addition, a probable fast moving asteroid was identified. The objects presented here are natural candidates for follow-up spectroscopic observations and illustrate the usefulness of the EIS data for a broad range of science and for providing possible samples for the first year of the VLT.

**Key words:** surveys — quasars: general — white dwarfs — stars: low-mass

### 1. Introduction

The present paper is the fourth of a series presenting the data accumulated by the public ESO Imaging Survey (EIS), being carried out in preparation for the first year of regular operation of the VLT. As described in previous papers (Renzini & da Costa 1997; Nonino et al. 1998, hereafter Paper I) the main goals of the EIS project are to conduct an imaging survey suitable for finding “rare” objects for follow-up observations with the VLT and to lay down the groundwork for more ambitious wide-field digital, multicolor imaging surveys. The adopted strategy was designed to search for distant clusters of galaxies, quasars, high-redshift galaxies and to identify rare stellar types.

As part of EIS-wide, observations were obtained in three passbands ( $B$ ,  $V$  and  $I$ ) over an area of about 1.7 square degrees in a region near the South Galactic Pole (EIS-wide patch B). The region was selected because of the high density of known intermediate red-shift quasars. The multicolor data for patch B are now being released and in a separate paper the observations, calibration and the overall quality of the data are described (Prandoni et al. 1998, Paper III). In that paper, preliminary single passband catalogs were presented and evaluated by comparing the star- and galaxy-counts with models and results from other surveys and the EIS patch A, presented in Paper I. The good agreement found from these

---

Send offprint requests to: M. Nonino

<sup>★</sup> Tables 2 to 8 are only available in electronic form at the CDS via anonymous ftp to cdsarc.u-strasbg.fr (130.79.128.5) or via <http://cdsweb.u-strasbg.fr/Abstract.html>

comparisons indicates that the available data, reduction procedures and object catalogs extracted in each of the passbands are reliable. Furthermore, comparison of the observed color distribution for point-like sources, derived from a preliminary version of a color catalog, with predictions of galactic models also shows reasonable agreement.

Although encouraging, the above results do not fully characterize the color catalog, in particular if it is to be used to identify different types of objects based on color selection criteria. Target selection based on the location of objects in color-color space, require a careful investigation of the performance of the pipeline since any problem may lead to objects with spurious colors. Colors are sensitive to a number of effects such as the observing conditions, the photometric and astrometric solutions in the different passbands and the de-blending algorithm. In order to have a better understanding of the impact of these effects in the color catalog, in this paper the  $(B - V)$  versus  $(V - I)$  diagram for point-sources is used to select objects lying in potentially interesting regions of the color-color space; such regions have been defined following by an appropriate modelling of the expected colors of such interesting objects. The objects, examined individually, are used to generate lists of candidates for different type of objects.

The goals of the present paper are: 1) to test the performance of the EIS pipeline in the production of object catalogs; 2) to assess the reliability of the color catalogs being extracted from the EIS multicolor data; 3) to provide ESO users with lists of potential VLT targets.

In Sect. 2, the basic characteristics of the color catalog relevant to the present work are described. In Sect. 3, the color-color diagram for point-like sources is inspected and empirical color criteria are used to generate a preliminary list of candidate white-dwarfs, low mass stars and quasars, with a range of red-shifts. Results and the outlook for the future is presented in Sect. 4.

## 2. The point-source color catalog

The color catalog described here has been constructed from objects detected in the 150 s exposures using multicolor data presented in Paper III. Color catalogs extracted from the co-added images will only be available in the final release.

As discussed in Paper III, the generation of a color catalog for generic use is a complex task given the range of possibilities in its definition, which depends to a large extent on the science goals. Since the intention of the present paper is primarily to understand some general characteristics of the color catalog and evaluate its usefulness for the primary science goals of the survey, the following prescription has been adopted. Starting from the unique catalogs covering the whole patch extracted from the best available images in each passband (see Paper III), a color catalog is created by associating the objects detected in the different passbands (see Paper I). The final product is a unique

entry for each object, listing the photometric parameters and flags for each detection in each passband, and information about the best seeing frames in all bands. This information allows limits on the color for objects not detected in some of the passbands to be calculated. At this point all detections are considered, regardless of the band in which they were detected and the nature of the object (star/galaxy).

It has been found, for instance, that this catalog contains objects detected in the blue passbands without counterparts in  $V$  and  $I$ . Visual inspection of some of these cases, which represent roughly 2% of the total number of objects for  $B \lesssim 22$ , shows that the unusual colors observed come mostly from objects detected at the border of individual frames or along diffraction spikes of bright stars. Others are due to ghost images present in the  $B$  and  $V$  images (see Paper III) and to merged images that are de-blended in some passbands and not in others, depending on the seeing. Even though this is the most general color catalog, it is not the most convenient catalog to use. This is especially the case for extended objects for which are contaminated by the problems mentioned above and for which one would like to have the object centroid and measure magnitudes with the same aperture in all bands. Another problem is that the star/galaxy classification may vary from band to band, thus implying that the object classification may not be unique.

To avoid some of these ambiguities, this paper considers only point-sources as defined in the  $I$ -band where image quality is more homogeneous than in other bands and it was preferred to the  $V$ -band (where image quality is slightly better Figs. 1 and 3 of Paper III), for consistency with the other patches and because the interest is mainly red objects. The selected sample includes only objects detected in the  $I$ -band brighter than  $I = 23.0$  and with SExtractor stellarity index  $\geq 0.75$ . In addition, all objects with non-zero SExtractor and WeightWatcher flags (Paper I) are removed from the catalog, in order to minimize contamination by spurious extreme color objects, which originate from some of the cases described above. It is worth pointing out that by eliminating all these objects a priori may discard some interesting cases. The final sample is available at <http://www.eso.org/eis/>.

Note that star/galaxy classification is only reliable for magnitudes brighter than  $I \sim 21.5$  and colors were computed using the `mag_auto` estimator introduced in Paper I. The mean error in the colors are less than 0.15 mag for sources brighter than the star-galaxy separation limit, and about 0.4 mag near the limiting magnitude of the sample.

Since the primary goal of this paper is to illustrate the possible use of EIS data for different science goals and to evaluate the size of interesting samples for follow-up work, the criteria adopted have been in general conservative. In particular, in the selection of targets discussed below only reliable  $I$ -band detections, with the error ( $\epsilon_I$ ) on the  $I$ -band magnitude  $\epsilon_I \lesssim 0.2$  ( $(S/N)_I \gtrsim 5$ ) are considered.

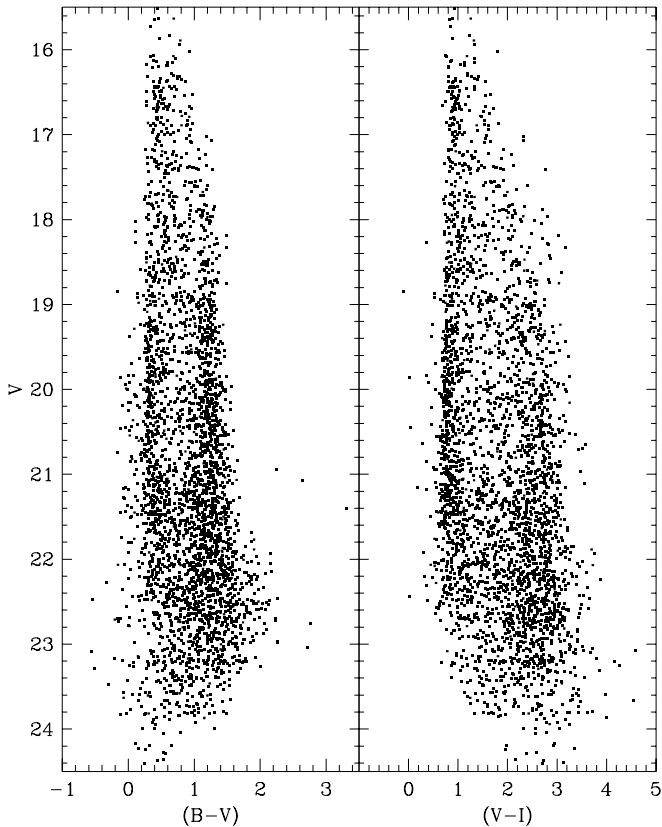


Fig. 1. Color-magnitude diagrams for EIS point-like sources

Furthermore, to avoid regions of very poor seeing and low transparency, some regions were discarded, based on the distributions of seeing and limiting isophotes shown in Paper III, leading to a sample covering a total area of 1.27 square degrees (e.g., Fig. 4). In particular, it was excluded the region with  $\alpha > 12^{\circ}75$ ,  $\delta > -29^{\circ}5$  with  $B$  and  $I$ -band seeing  $> 1''.3$ , and the region  $12^{\circ}10 < \alpha < 11^{\circ}90$ ,  $\delta < -29^{\circ}75$  with limiting isophote in  $I$ -band  $\lesssim 25$  (very poor transparency).

To illustrate the general properties of the sample the color-magnitude diagrams  $V$  versus  $(B - V)$  and  $V$  versus  $(V - I)$  are shown in Fig. 1 for 3233 point-sources with  $S/N \gtrsim 5$  in the  $I$  passband. The color distribution for sources brighter than  $V = 21$  has already been discussed in Paper III and compared with model predictions. This plot is presented in  $V$ -band to make the comparison with other works easier (e.g., Reid & Majewski 1993). Note that at faint magnitudes ( $V \gtrsim 21.5$ ) incompleteness in the stellar sample sets in (see Paper III). In the figure blue,  $(B - V) \sim 0.5$ , and red,  $(B - V) \sim 1.5$  concentrations are clearly seen for  $V \gtrsim 18.5$ . This reflects the typical bimodal color distribution observed for faint stars at high-galactic latitude, with the blue peak arising from the turnoff of the main sequence for low-metallicity halo stars and the red peak from disk stars. Note that the blue peak is well-defined in the magnitude range  $18.5 < V < 21.5$ .

For fainter magnitudes it fades away partly due to the incompleteness of the catalog and partly because at this magnitude limit one is approaching the outer parts of the halo.

From the figure one sees that for  $V \gtrsim 19$  there is a large number of objects bluer than the concentration associated with the halo stars, and for  $V \gtrsim 21.5$  there is a population of very red objects with  $(V - I) > 3.5$ . Both are examples of interesting populations, the identification of which is better explored using the color-color diagram as discussed in the following section.

### 3. Target selection

Figure 2 left panel shows the color-color diagrams for the 3233 point sources detected simultaneously in the  $B$ ,  $V$  and  $I$  band with  $(S/N)_I \gtrsim 5$ ; Fig. 2 right panel shows the 345 objects only detected in  $V$  and  $I$  and not in  $B$ -band with  $(S/N)_I \gtrsim 5$ . The plots include all objects brighter than  $I = 23$ . For non-detections in  $B$  (hereafter  $B$ -dropouts) an estimate of the  $B$  limiting magnitude has been measured on the best seeing frame. The limiting magnitude is defined to be a  $1\sigma$  detection within the area corresponding to the seeing-disk as measured in the  $I$ -band. From this an estimate of the lower limit on the  $(B - V)$  color is calculated. In addition to the  $B$ -dropouts, there are objects only detected in the  $I$ -band, for which the lower limit in  $(V - I)$  is similarly computed. While a large number of these objects is expected if one considers the sample as a whole (because of the relative bright limiting magnitudes of the  $V$  images), objects brighter than  $I \sim 21$  are the most interesting and are the ones considered in more detail below.

For comparison with the previous figures, Fig. 3 shows the locus of main sequence, giants, white dwarf and brown dwarf stars. The stellar locus for main sequence, subgiant- and red-giant branch stars typical of the old low-metallicity halo and the young solar-type metallicity disk was taken from the models of Bertelli et al. (1994) extending down to  $0.6 M_{\odot}$ . The color-color cooling sequence for pure-Hydrogen WD was taken from Bergeron et al. (1995). Finally, the locus for very low mass stars and/or brown dwarfs down to  $0.08 M_{\odot}$  is taken from the models of Baraffe et al. (1998). These curves are presented in the Jonhson-Cousins system, close to the EIS magnitude system except for the  $B$ -band (Paper III). However, the differences are relatively small and have no significant impact on the adopted selection criteria described below.

Also shown in Fig. 3 is the track of quasars in the color-color diagram as a function of redshift and the typical color scatter along the sequence due to the different assumptions for their typical spectra and intervening absorption. QSO colors were simulated using synthetic QSO spectra, which cover a range of intrinsic spectral properties, and the response functions of the EIS

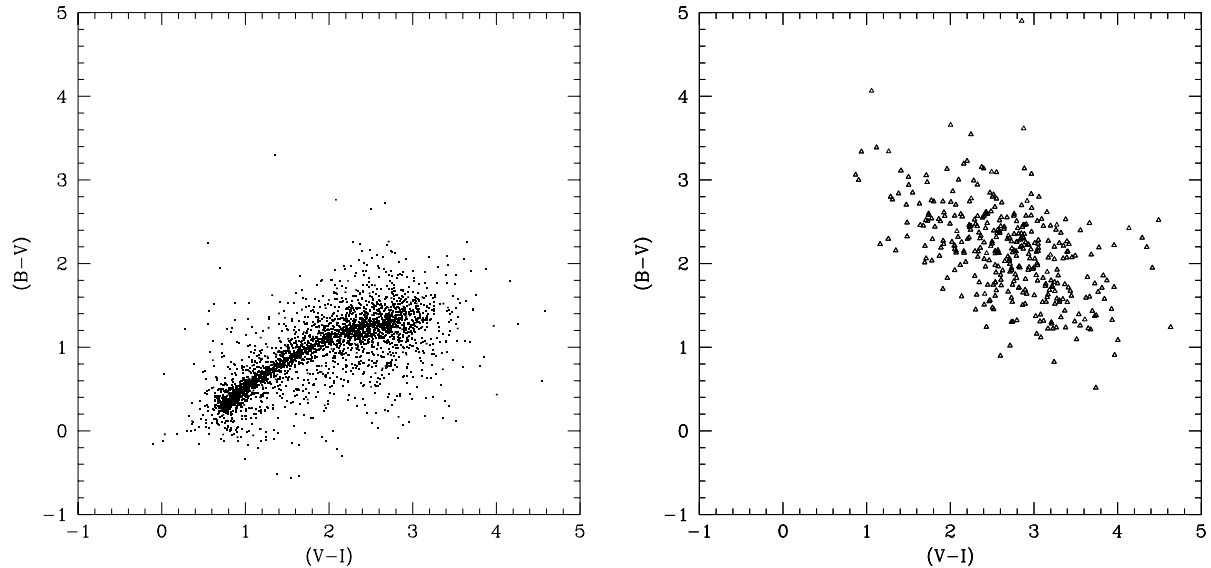


**Fig. 2.** Color-color diagram for EIS point-sources. Left-panel: those detected in all three passbands. Right-panel: those detected in  $V$  and  $I$  but not  $B$ , for which the lower limit in  $(B - V)$  is indicated

**Table 1.** Definition of regions of interest in Fig. 3 for candidate objects

Region	Cand. Objects	Definition
I	VLM/BD	$(V - I) \geq 3.5$
II	WD	$(V - I) \leq 0.5$ and $(B - V) \leq 0.5$
III	QSO	$\begin{cases} -0.25 < (V - I) < 0.5 \text{ and } (B - V) > 0.5 \\ 0.5 < (V - I) < 2.0 \text{ and } (B - V) > 0.86(V - I) + 0.29 \\ 2.0 < (V - I) < 3.5 \text{ and } (B - V) > 2.0 \end{cases}$
IV	QSO Low $z$	$0.5 < (V - I) < 1.0$ and $-0.25 < (B - V) < 0.25$

filters (Paper I). The method is the same as that used by Warren et al. (1994) and Hall et al. (1996), and is a modified version of the method of Warren et al. (1991). QSO spectra were synthesised assuming that the QSO continuum has the form of a single power law with spectral index  $\alpha$  ( $S(\nu) \propto \nu^\alpha$ ) and assuming fixed emission line strengths relative to  $\text{Ly}\alpha + \text{NV}$ . Three different values of the spectral index  $\alpha = (-0.25, -0.75, -1.25)$  were used, and three different values for the emission line strength, defined by the  $\text{Ly}\alpha + \text{NV}$  rest-frame equivalent width,  $\text{EW}(\text{Ly}\alpha + \text{NV}) = (42, 84 \text{ and } 168 \text{ \AA})$ . For each set of assumptions, spectra were generated at intervals of 0.1 in  $z$  over the range ( $3.0 < z < 5.0$ ). Absorption by intervening HI was taken into account by simulating absorption spectra, following the method of Warren et al. (1994) and based on the work of Møller & Jacobsen (1990). For each set of intrinsic properties, ten QSO spectra were generated at each  $z$  step, each using a different realization of the absorption spectrum appropriate for that redshift. Thus at each redshift a total of 90 spectra were generated. Because patch B is close to

the South Galactic Pole galactic extinction was neglected in the present calculation. Figure 3 shows the median and the scatter corresponding to the various simulations as a function of redshift.

In addition, in Fig. 3 all the 19 known quasars present in the field are shown in their measured EIS magnitudes. These quasars have redshifts, taken from the literature, in the range  $0.4 < z < 2.96$ .

Comparison of the color-color diagram for the data and model predictions shows at least four regions of potential interest. These regions are schematically shown in Fig. 3 and their limits are given in Table 1. Objects in region I are candidate very low mass stars (VLM) or brown dwarf stars (BD), those in region II are candidate white dwarfs (WD). Candidate quasars (QSO) at different redshifts should lie in regions III and IV. Below preliminary lists for these objects are presented in tables which give: in Col. (1) the object name; in Cols. (2) and (3) the J2000 coordinates; in Cols. (4) and (5) the  $I$  magnitude and its error estimate  $\varepsilon_I$ ; in Cols. (6) and (7) the  $(B - V)$  color and its error estimate  $\varepsilon_{(B-V)}$ ; in Cols. (8) and (9) the

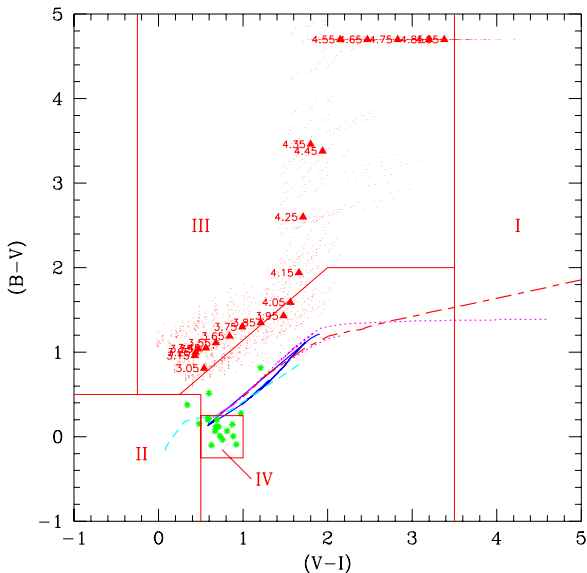


**Fig. 3.** Theoretical color-color plot for different type of objects. The solid line shows the location of main sequence, sub- and red-giant branch stars of an old halo, low metallicity, stellar population model taken from Bertelli et al. (1994). The dotted line shows the location of main sequence, sub- and red-giant branch stars of a young disk, solar metallicity, stellar population model taken from Bertelli et al. (1994). The short-dashed line shows the location of a WD pure Hydrogen cooling sequence taken from Bergeron et al (1995). The long-dashed line shows the location of 5 Gyr old BD stars with solar metallicity, taken from Baraffe et al. (1998). The color track for QSOs at different redshifts ( $3.05 < z < 5.00$ ) are shown by triangles while the dots indicate the typical scatter around the median for the different parameters of the spectral properties and absorbers of high-redshift quasars (see text). Also shown (stars) are the EIS colors of the known quasars present in the EIS catalog which have redshifts in the range  $0.4 < z < 2.96$

$(V-I)$  color and its error estimate  $\varepsilon_{(V-I)}$ ; and in Col. (10) notes or comments on the individual objects, whenever necessary. In the cases where the  $(B-V)$  and/or  $(V-I)$  colors are lower limits, the measure is preceded by a  $>$  sign and the error in the color is the error in the magnitude in the passband in which the object is detected. For objects not detected in two passbands the error in the color is set to zero in the tables.

### 3.1. Rare stellar-type candidates

One of the interesting regions of the color-color diagram is the region redder than  $(V-I) \geq 3.5$  (region I). Objects in this region extend well beyond the track defined by main-sequence stars with masses greater than  $0.6 M_{\odot}$ . Therefore, this region should be populated primarily by

very low mass stars ( $0.6 > M/M_{\odot} > 0.1$ ) in the disk and/or brown dwarfs. Another possibility is that they are asymptotic giant and red giant branch stars. However, this is unlikely because there should be few of them in this color and magnitude range since they would have to be high metallicity objects at very large distances from the Sun ( $\sim 100$  kpc). Even though unlikely, considering the size of the area covered by the EIS multicolor data, this region of the color space could also be populated by very high-redshift QSOs with very large  $(B-V)$ , which could appear as  $B$  non-detections. In this region there are 18 detections (listed in Table 2; 22  $B$ -dropouts with  $(V-I) \geq 3.5$ , all brighter than  $I = 20$  (listed in Table 3); and 14 objects with  $I \lesssim 21$ , which are only detected in the  $I$ -band (listed in Table 4). In the tables with “rare” stellar objects (2, 3 and 4), the following naming convention has been adopted: VLM, for very low mass candidates, VLMB, for very low mass  $B$ -dropouts, and VLMI, for the objects only detected in the  $I$ -band.

Since extreme colors could be caused by some unexpected artifact all these cases have been visually inspected, and all seem to be legitimate candidates. Note, however, that in the course of the inspection the two brightest objects in this sample exhibited a strange morphology in the coadded image appearing to be a “double” star, with the two objects having almost exactly the same magnitude,  $I = 17.46 \pm 0.01$ , and a few arcsecs of separation. This prompted the examination of the two single frames, which showed a single slightly elongated object that occupies different positions in the two single exposure images. The object was observed at  $\alpha = 00^{\text{h}}49^{\text{m}}37^{\text{s}}.71$ ,  $\delta = -29^{\circ}50'58''.7$ ,  $\text{JD} = 50696.3174202$  and  $\alpha = 00^{\text{h}}49^{\text{m}}37^{\text{s}}.76$ ,  $\delta = -29^{\circ}50'56''.7$ ,  $\text{JD} = 50696.32054438$ . This fact strongly suggests that this object is probably a relatively fast moving asteroid. However, no known asteroids were found to be at the observed position during the nights the observations were conducted. This example of a serendipitous source demonstrates the need to implement tools in the EIS pipeline to search for transient phenomena present in the survey such as high proper-motion objects, variables, supernovae.

Another potentially interesting population is that defined by objects in region II of Fig. 3. These objects are clearly visible in Fig. 1 at magnitudes  $V \gtrsim 19.5$ . These blue objects could be either relatively hot (young) disk white dwarfs or blue horizontal branch (HB), low-metallicity halo stars. However, for  $V \gtrsim 20$  HB stars would be located at  $\gtrsim 100$  kpc, where the density should be extremely small for standard galactic structure models. There are 32 objects in region II which are listed in Table 5. The adopted cut-off in  $(V-I)$  (see Table 1) was chosen based on cooling sequence of disk white dwarfs (Bergeron et al. 1995) shown in Fig. 3. We emphasize that the criterion adopted is somewhat arbitrary and it is used simply to illustrate the possible identification of these

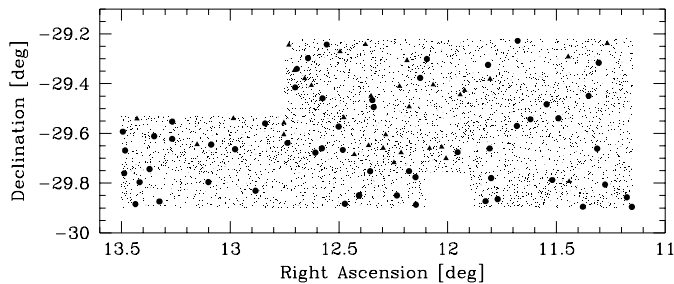


**Fig. 4.** Projected distribution of star-like objects which shows: all stellar objects detected in the selected area of patch B (dots); low-mass candidates found in region I of the color-color diagram of Fig. 3 (filled circles); and WD candidates in region II (filled triangles)

objects. As can be seen from Fig. 3, this sample can be contaminated by low redshift quasars. In fact Table 5 contains 2 already known quasar which are identified (name and redshift from the Simbad database). The  $U$ -band data will be useful to sort out these cases.

Finally, Fig. 4 shows the spatial distribution of these various candidates. Note that the northeast edge of the patch has been removed because of the incompleteness of the  $B$ -band catalogs. Similarly, a region along the southern edge was removed because of the incompleteness in the  $I$ -band catalog. A small trimming of the whole region has also been done yielding a total area of 1.27 square degrees.

### 3.2. Quasar candidates

From simulations of QSO tracks (Fig. 3) high redshift QSOs ( $3 < z < 5$ ) can be found in region III of the color-color diagram, while the available sample of known low redshift QSOs populate region IV (see Fig. 3, Osmer et al. 1998). The rough criteria used to define region III (Table 1) were chosen based on the simulated QSO track. The blue part was chosen to be parallel to the stellar locus but shifted to minimize the contamination by stars. Several improvements in the selection can be made to take into account the errors in colors, as a function of the magnitude, and to optimize the yield based on the expected density of objects of different types. Since the parent sample is public, interested groups are likely to make significant refinements to the selection criteria adopted here.

In region III there are 70 objects detected in all three passbands. These are listed in Table 6. In addition, there are 126 objects that are detected in  $V$  and  $I$  but not detected in  $B$  (hence have lower limits in  $(B-V)$ ) that could also lie in region IV. These objects are listed in Table 7. Note that, since the depth of the  $B$  images varies across the patch, the limits on  $(B-V)$  are more meaningful in some areas than others. The depth of the  $B$  frames cor-

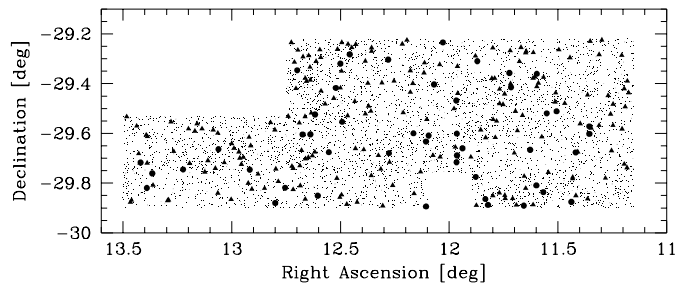


**Fig. 5.** Projected distribution of quasar candidates at low (filled circles), intermediate and high redshift (filled triangles). The adopted selection criteria are discussed in the text

responding to each object can be calculated from the  $V$  magnitude and the  $(B-V)$  limits given in Table 6. In the tables the following naming convention has been adopted: QSO and QSOB stand for objects in region III detected in all three bands ( $z \gtrsim 3.0$ ) and  $B$ -dropouts candidates, respectively.

Adopting the criteria given in Table 1 for region IV, where QSOs with  $z \lesssim 3$  are likely to be found, one finds 48 stellar objects which are listed in Table 8. This table includes 6 known QSOs, as indicated (name and redshift are from the Simbad database). In the table QLZ stands for low redshift ( $z \lesssim 3.0$ ) quasars. Note, however, that with the follow-up observations in  $U$ -band to be carried out later this year, it will be possible to select low- $z$  QSOs more efficiently.

Figure 5 show the projected sky distribution of the QSO candidates. This figure should be compared with those for the seeing and the limiting magnitudes presented in Paper III to investigate possible correlations between the QSO candidates and the quality of the data, especially the  $B$ -dropouts or those detected only in the  $I$ -band. At first glance there is no obvious correlation as the QSO candidates seem to be uniformly distributed over the surveyed area.

## 4. Summary

The ESO Imaging Survey is being carried out to help the selection of targets for the first year of operation of VLT. This paper presents some examples of possible candidates of interest, giving special emphasis to stellar populations and quasars. Using the area covered by the survey one is able to find candidate WDs and red objects likely to be associated with very low mass stars or brown dwarfs. A preliminary list is also presented for quasars. These lists and image postage stamps in all three passbands are also available in the ESO Science Archive server which allows the examination of the candidates ("<http://www.eso.org/eis/>"). Finding charts can also be easily extracted. Also available is the parent color sample from which these candidates have been

defined. It is important to emphasize that in addition to providing these preliminary lists, the present work has been an essential part in understanding the characteristics of the color catalogs being produced and for the verification of their reliability.

Improvements in the sample selection are certainly possible. The combination of Galactic models, stellar evolution, quasar properties and an appropriate modelling of the observational errors in principle can lead to the definition of some probability function that can be better used to identify interesting objects; another way can be a direct fit to the broadband spectral emission of the objects. This is beyond the scope of this paper and since the data are publicly available, interested groups may refine the selection criteria and produce their own samples. The present results lead to samples that are of the order of 50 to 100 candidates each. The yield will only be defined by follow-up spectroscopic observations. Much larger samples will be available from the Pilot Survey to be carried out with the new Wide Field Imager at the 2.2 m telescope at La Silla.

Finally, it has been communicated that observations performed at the 2dF of a sample of bright QSO candidates presented in this paper resulted in an identification of 14 QSO with redshift in the range  $1 \div 2.2$  out of 26 candidates with a success rate above  $\sim 50\%$  (S. Cristiani, private communication).

*Acknowledgements.* We thank all the people directly or indirectly involved in the ESO Imaging Survey effort. In particular, all the members of the EIS Working Group for the innumerable suggestions and constructive criticisms, the ESO Archive Group and the ST-ECF for their support. Special thanks to A. Baker and D. Clements for their contribution in the quasar search in the early stages of the EIS

project. We would like to thank S. Warren for helpful comments and providing the code for the calculation of the color track for quasars for the EIS filters and I. Baraffe for providing the locus of brown dwarfs in the appropriate passbands. We would also like to thank R. Saglia, B. Boyle, M. Colles and S. Cristiani for communicating their results before of publication. Our special thanks to the efforts of A. Renzini, VLT Programme Scientist, for his scientific input, support and dedication in making this project a success. Finally, we would like to thank ESO's Director General Riccardo Giacconi for making this effort possible in the short time available. This research has made use of the Simbad database, operated by the Centre de Données astronomiques de Strasbourg.

## References

- Baraffe I., Chabrier G., Allard F., Hauschildt P.H., 1998, *A&A* 337, 403  
 Bertelli G., Bressan A., Chiosi C., Fagotto F., Nasi E., 1994, *A&ASS* 106, 275  
 Bergeron P., Wesemael F., Beauchamp A., 1995, *PASP* 107, 1047  
 Boyle B.J., 1989, *MNRAS* 240, 533  
 Hall P.B., Osmer P.S., Green R.F., Porter A.C., Warren S.J., 1996, *ApJ* 462, 614  
 Møller P., Jakobsen P., 1990, *A&A* 228, 299  
 Nonino M., Bertin E., da Costa L., et al., 1999, *A&A* 137, 51 (Paper I)  
 Osmer P.S., Kennefick J.D., Hall P.B., Green R.F., 1999, *ApJS* 119, 1890  
 Prandoni I., et al., 1999, *A&A* (submitted) (Paper III)  
 Renzini A., da Costa L., 1997, *The Messenger* 87, 23  
 Reid N., Majewski S.R., 1993, *ApJ* 409, 635  
 Warren S.J., Hewett P.C., Osmer P.S., 1994, *ApJ* 421, 412  
 Warren S.J., Hewett P.C., Irwin M.J., Osmer P.S., 1991, *ApJS* 76, 1